Effect of Electric Field on Water Confined in Graphite and Mica Pores

Rajat Srivastava,[†] Jayant K. Singh,*,[†] and Peter T. Cummings[‡,§]

[†]Department of Chemical Engineering, Indian Institute of Technology Kanpur, Kanpur 208016, India

[‡]Department of Chemical and Biomolecular Engineering, Vanderbilt University, Nashville, Tennessee 37235, United States

[§]Center for Nanophase Material Sciences, Oak Ridge National Laboratory, Oak Ridge, Tennessee 37831-6494, United States

ABSTRACT: We examined the influence of external electric field on the vapor–liquid coexistence curve and on structural properties of TIP4P/2005 water confined in hydrophobic and hydrophilic pores using all-atom molecular dynamics simulations. While the electric field increases the critical temperature of bulk water, the effect is contrary on the confined water. We clearly observe that the critical temperature of confined water decreases with increasing field strength. The current work strongly indicates that using electric field results in a decrease in the saturated liquid phase density and increase in the saturated vapor phase density of the confined water and can be used to modulate the evaporation rate of water under confinement. The effect of an electric field on the confined fluids is more pronounced at higher temperature. We also report that the critical density of water behaves differently in hydrophobic and hydrophilic pores. With increasing electric field, the critical density increases in hydrophobic pores; however, it is found to decrease in hydrophilic pores. We analyze the results using pair correlation functions and orientational, tetrahedral, and hydrogen bond distributions. Our investigation indicates that the presence of an electric field enhances the coordination number $N(r)$ of the bulk phase. In contrast, the presence of an electric field reduces $N(r)$ of the confined fluid. This is clearly reflected in the behavior of the critical temperature of bulk and confined water. Our structural analysis reveals that the application of an external field induces orientational order of dipole vector parallel to the field direction in bulk water, whereas its effects on dipole orientation is much less in confined systems. We also report that the hydrogen-bonding behavior in the vapor phase is responsible for the difference in critical density of water confined in hydrophobic and hydrophilic pores.
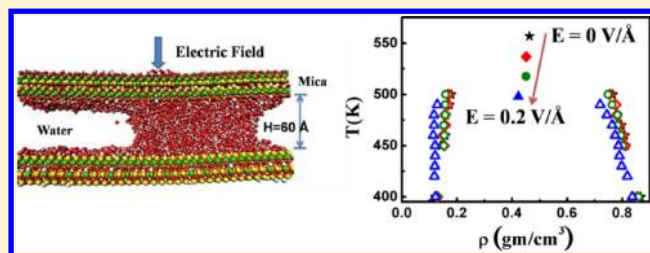
1. INTRODUCTION

Nanoscale properties of fluids are significantly affected by the surfaces.[1–4] For example, vapor–liquid phase transitions of fluids undergo a crossover from 3D to 2D phase transition under confinement.[1,3,5–8] The presence of confining surfaces causes depression in critical temperature and structural changes and may lead to entirely new phenomena. The knowledge of vapor–liquid phase transition under confinement is relevant to reaching fundamental understanding thermophysical properties of fluids as well as advancing technology. For example, nano/micro pumps can be designed based on thermally driven liquid–vapor phase change.[9–11] The advantage of these nano/micro pumps[12] is that they do not require mechanical moving parts for actuation and use the difference in surface tension or viscosity between the vapor and liquid phase of a confined fluid to actuate the flow in nano/micro channels.

In addition to confining surfaces, external fields—such as electric and magnetic fields—can also dramatically change the phase behavior of confined water, which is not well understood. Recent interest has grown in understanding the influence of external fields on fluids due to their wide application in many fields such as in chemical processes such as electrophoresis and electrofilteration. The growth in the fields of nanotechnology and nanobiotechnology has significantly opened the door for practical applications of confined fluids in the presence of external fields for nanomaterials synthesis, nanofluidics, and field-controllable drug delivery. Electrospinning[13,14] is a novel textile manufacturing technology used for making nanofibers which are generated by an electrified jet (composed of nanoconfined viscous polymer solution inside an electrified nozzle tip). The nanofibers are continuously stretched because of the electrostatic repulsions between the nozzles surface charges and the evaporation of solvent. The process of electrospraying[15] is also similar to electrospinning and can be used in many applications, including inkjet printing, mass spectroscopy, and nanoparticle deposition for patterning of polymer films. It is important to note that water is the most prominent solvent component in many electrospraying processes; therefore, the influence of a strong electric field on the water solvent is of broad scientific and technological interest.

Several experimental studies have been performed to understand the effect of external fields on vapor–liquid and liquid–liquid phase transitions, with conflicting results. Originally Debye and Kleboth[16] predicted a shift of the critical temperature for the binary system of isooctane/nitrobenzene as a result of the application of external electric field. They reported that the application of electric field of the order of

10^{-4} V/Å decreases the critical temperature of the binary system by several mK. These results are further verified by Orzechowski,[17] who concluded that the decrease in critical temperature is proportional to the square of electric field. The work of Debye and Kleboth has been followed by Beaglehole,[18] who investigated the effects of electric field on critical behavior of binary mixture of cyclohexane/aniline. They observed the downward shift in the critical temperature of the binary system. Early[19] also worked on the same system (cyclohexane/aniline) and reported no sign of change in critical temperature of the system, which contradicts earlier experiments.[16,18] Early reported that the discrepancy in the results is due to the presence of electric field which causes local heating in the binary system. Hegseth and Amara[20] also observed an increase in critical temperature of SF_6 of several mK on application of electric field of strength 10^{-5} V/Å. The electric field not only affects the critical temperature of the system but also influences a wide range of thermophysical properties. A recent experimental study conducted by Bateni et al.[21] shows that the application of an electric field causes an increment in the contact angle of the alcohols and alkanes on a Teflon-coated silicon wafer surface.

Molecular simulation is a powerful molecular probe for understanding thermophysical phenomena. Several simulation studies have also been performed in order to investigate the influence of an electric field on vapor−liquid phase transition,[22−24] finding that the application of an electric field enhances the bulk critical temperature. Recently, Maerzke et al.[25] examined the influence of an electric field on the vapor−liquid coexistence curve of bulk water, methanol, and dimethyl ether, reporting that there is increase in critical temperature of about 3% on application of $E = 0.1$ V/ Å in comparison to zero electric field. Okuno et al.[13] reported that the evaporation of water can be enhanced by the application of an electric field in the direction perpendicular to the liquid−gas interface, while it impedes the evaporation when electric field is applied in parallel direction to the liquid−gas interface of water. Yeh and Berkowitz[26] using molecular dynamics simulation on water in the presence of high electric field observed that the dielectric constant of water decreases with increasing electric field.

In addition to the bulk fluid, the role of external field on a fluid under confinement has also attracted many workers. Recently, Zhang et al.[27] studied the freezing transition of water in hydrophobic nanoconfinement under the influence of an external magnetic field, reporting a new phase of bilayer crystalline ice at a freezing temperature of 340 K. They also reported that the magnetic field increases the freezing temperature of the water under confinement. Svischev and Kusalik[28] performed molecular dynamics (MD) simulations and reported the presence of electric field near the surfaces or within the confined geometries can play an important role in the crystallization of liquid water. The interest is not only limited to freezing/melting transition of confined fluids but includes a wide range of macroscopic properties. Application of an electric field on a confined system can be used to influence thermophysical properties including wettability,[29,30] adhesion, and friction[31] for nanofluidics as well as vapor−liquid transition. Vaitheeswaran et al.[32] performed MD simulations to study the effect of an electric field on water confined between two hydrophobic plates in an open system. Their results reveal that the presence of electric field decreases the density of confined water film, and it also enhances evaporation of confined water. This trend is in the opposite direction to the prediction

obtained from the bulk thermodynamics of electrostriction (the term is used usually to describe the densification of water in the presence of an electric field generated by an ion). Vaitheeswaran et al. also reported that the free energy barrier for capillary evaporation of water confined between the plates is reduced by the application of an electric field. On the other hand, the results of Bratko et al.[33,34] are contradictory in nature, where they reported that the nanoconfined water shows the usual phenomena of electrostriction, i.e., increase in density of the liquid phase confined in hydrophobic pores with increasing electric field. England et al.[35] made an attempt to addresses the above contradictory observations using mean-field theory. They reported that the lowering of density of the confined water has been observed at lower electric field strengths ($E = 0−0.2$ V/ Å), where the alignment of water molecules with the applied electric field reduces due to geometric frustration in hydrogen bonding because of the confinement, whereas higher electric field (above 0.6 V/Å) aligns the water molecules between the plates, leading to increased density. Zhu and Robinson[36] also studied the influence of an electric field on hydrogen bonding in water confined between plates and reported that the enhancement of electric field results in the alignment of water molecule near the surface, leading to the breaking of hydrogen-bonding network near the confining surfaces.

Despite these (in some cases conflicting) studies, a number of key issues remain unaddressed. For instance, the effect of an electric field on vapor−liquid or liquid−solid phase transitions, and in particular on pore critical temperature, of nanoconfined water and other polar molecules between hydrophobic and hydrophilic surfaces is not clear. To the best of our knowledge, phase transitions and critical properties under structured nanopores in the presence of an electric field have not been previously studied. Therefore, in the current work, we present MD simulations probing the effect of an electric field on vapor−liquid phase transition, using all-atom molecular dynamic simulation of water confined in graphite (hydrophobic) and mica (hydrophilic) slit pores.

2. SIMULATION DETAILS

2.1. Potential Model. The TIP4P/2005 model is used for the water−water interaction,[37] the interaction parameters for graphite−water ($\sigma_{co} = 3.262$ Å and $\varepsilon_{co} = 0.0926$ kcal/mol) are those used by Koga et al.,[38] and a fully flexible atomistically detailed model[39,40] (Table 1) of the mica surface consisting of

Table 1. Force Field Parameters for Mica Surface[39]

I. nonbonded	charge	σ (Å)	ε(kcal/mol)
K	+1.0	3.385 42	0.20
Si^{surface}	+1.1	3.563 59	0.05
Al^{surface}	+0.8	3.741 78	0.05
Al^{octahedral}	+1.45	3.741 78	0.05
O^{surface}	−0.55	3.118 15	0.025
O^{apical}	−0.758	3.118 15	0.025
O^{hydroxyl}	−0.683	3.118 15	0.025
H^{hydroxyl}	+0.20	0.978 296	0.013
II. bonds		l_0 (Å)	k_l (kcal/(mol Å^2))
all bonds between Si, O, Al		exptl[40]	860
O−H		0.929	990
III. angles		θ_0 (deg)	k_θ (kcal/(mol rad^2))
all angles between Si, O, Al		exptl[40]	340
H−O−Al		116.2	23

two mica sheets is used. The corresponding mica–water interaction parameters are calculated using the Lorentz–Berthelot mixing rule. Each graphite surface consists of two layers of carbon atoms separated by 1.53 Å with an interlayer separation of 3.4 Å. van der Waals interactions between atoms are described by the 12–6 Lennard-Jones (LJ) potential, and the particle–particle particle–mesh (PPPM) technique is applied to account for long-ranged electrostatic forces. Nonbonded interactions are described by a combination of Lennard-Jones (LJ) and Coulombic potentials

$$U_{nonbonded} = 4\varepsilon_{ij}\left[\left(\frac{\sigma_{ij}}{r}\right)^{12} - \left(\frac{\sigma_{ij}}{r}\right)^6\right] + \frac{q_i q_j}{4\pi\varepsilon_0 r_{ij}} \quad (1)$$

where ε_{ij} and σ_{ij} are the characteristic energy and size parameters, respectively, for the van der Waals interaction between atom i and atom j, q_i is the partial charge on atom i, ε_0 is the permittivity of free space, and r_{ij} is the distance between the centers of mass of the pair of atoms. All bonds between Si, O, and Al of the mica surface are described by harmonic potentials

$$U_{stretching} = \frac{1}{2}k_l(l - l_0)^2 \quad (2)$$

and

$$U_{bending} = \frac{1}{2}k_\theta(\theta - \theta_0)^2 \quad (3)$$

where k_l and k_θ are force constants and l, θ, l_0, and θ_0 are bond length, bond angle, and their corresponding equilibrium values, respectively.

The energy contribution from applied electric field is given by

$$u_{field} = -\sum_{i=1}^{N}\sum_{k=1}^{3} q_k(\mathbf{r_k}^i \cdot \mathbf{E}) \quad (4)$$

where $\mathbf{r_k}^i$ is the position vector of the kth point charge q_k of the ith molecule and $\mathbf{E}$ is the electric field applied to the system. In the current work, we apply the electric field in the z-direction only.

2.2. Simulation Method. MD simulations are performed using the LAMMPS[41] MD package, and periodic boundary conditions are applied along the unbounded directions x and y. We have considered water confined inside two parallel graphite or mica surfaces. The surfaces, separated by a distance H, are symmetric about the center of simulation box such that they are parallel to $x-y$ plane and equidistant ($H/2$) from the $z = 0$ plane. In this work, the distance between the pore walls, the pore width (H), are taken as 40 and 60 Å. We set up a simulation box of lengths L_x, L_y, L_z in the x, y, z directions, respectively. To accommodate the formation of vapor and liquid phases, we study the structural properties of confined water using MD simulations in the canonical (constant number of atoms N, constant volume V, and constant temperature T) ensemble with the Nosé–Hoover thermostat. Long-range interactions are treated using the particle–particle particle–mesh (PPPM) technique. The two-dimensional corrections have been employed in a similar way as used by Gordillo et al.[42] The equilibration time is set to be 0.5 ns with a time step of 0.001 ps, with production times of 0.5 ns.

The coexistence densities at a given saturation temperature are obtained by averaging the two-phase density ($\rho(x)$) profile over appropriate regions as reported in our earlier work.[1] The statistical error in the average densities is calculated from the standard deviation of block average densities. We have estimated the vapor–liquid critical parameter by fitting the coexistence densities, for a series of temperatures, to the law of rectilinear diameter[43] and the scaling law for the density.[44]

$$\rho_l - \rho_v = B\left(1 - \frac{T}{T_c}\right)^\beta \quad (5)$$

$$\frac{\rho_l + \rho_v}{2} = \rho_c + A\left(1 - \frac{T}{T_c}\right) \quad (6)$$

where ρ_l, ρ_v, ρ_c, T_c, and β are the liquid-phase density, vapor-phase density, critical density, critical temperature, and critical exponent, respectively, and A and B are fitting parameters. The errors in the coexistence densities and critical properties are found to be less than 1% and 2%, respectively.

Finally, we have investigated the effect of the electric field on the hydrogen-bonding (HB) distribution of confined water using the geometrical criteria as described by Swiatla-Wojcik,[45] since hydrogen bonding plays a vital role in determining the structural and dynamical behavior of water.

3. RESULTS AND DISCUSSION

Figure 1 illustrates the effect of applied electric field strength on the vapor–liquid phase diagrams of bulk water, water confined in graphite, and water confined in mica slit pores of width $H = 40$ Å. As shown in Figure 1, the liquid-phase density of bulk water increased with the applied electric field, whereas the vapor-phase density showed the opposite trend. Thus, the observed broadening in the vapor–liquid coexistence curve resulted in an increase in the critical temperature of bulk water, as previously reported by Maerzke et al.[25] and Argones et al.[46] The increase in bulk liquid-phase density of TIP4P/2005 water can be explained by the well-known thermodynamic expression of electrostriction, discussed by Kirkwood and Oppenheim[47] and Frank[48] and also recently reported by Vaitheeswaran et al.[32] It relates the change in the density of the fluid with the electric field E as

$$\frac{\rho(E) - \rho(0)}{\rho(0)} = \frac{\kappa_T^0 \rho(0)}{8\pi}\frac{\partial\varepsilon}{\partial\rho(0)}E^2 \quad (7)$$

where $\kappa_T = \kappa_T^0 + O(E^2)$ is the compressibility of the fluid, ε is the dielectric constant, and $\rho(E)$ and $\rho(0)$ are densities of fluid in the presence and absence of electric field E, respectively. This expression is applicable at low electric fields.

Equation 7 suggests that the density changes with the square of the electric field, and the sign of this change is determined by the sign of κ_T^0 and $\partial\varepsilon/\partial\rho(0)$. Molecular simulation studies by Gonzalez et al.[49] and Pi et al.[50] on bulk TIP4P/2005 water show that in the absence of electric field the dielectric constant increases with increasing density, and the isothermal compressibility $\kappa_T^0 > 0$; i.e., $\partial\varepsilon/\partial\rho(0)$ and κ_T^0 are positive. Therefore, we conclude that the density of liquid phase of the bulk TIP4P/2005 water increases with the increasing electric field, which in turn results in the increase in the critical temperature. This is in line with the analysis of Vaitheeswaran et al.[32] based on experimental studies.

The presence of confining surfaces is known to cause a reduction in the critical temperature of confined fluids as compared to that in the bulk state,[51] and this behavior has been
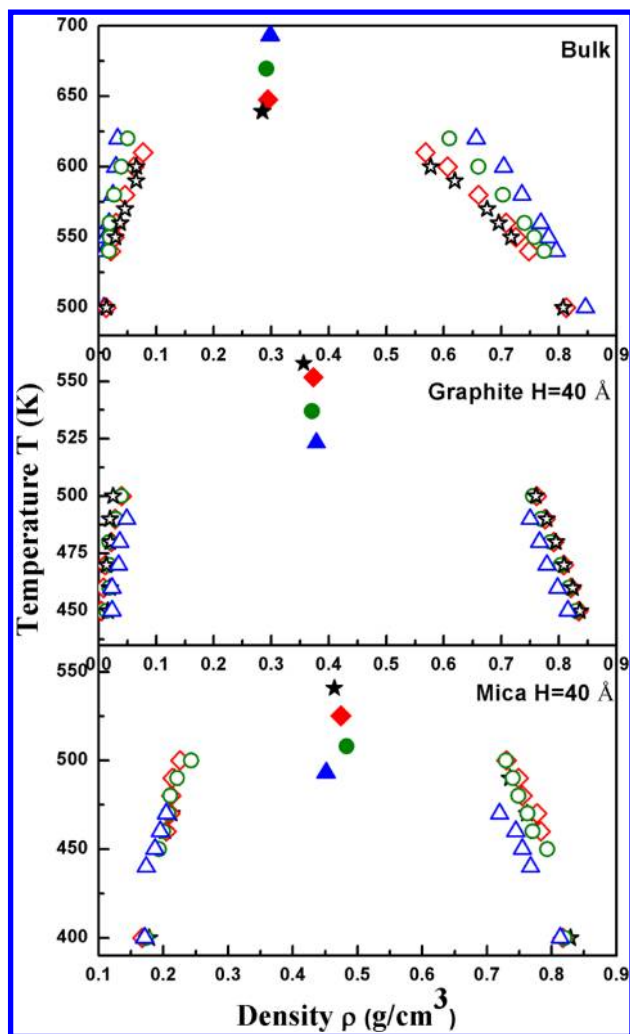
Figure 1. Vapor−liquid coexistence curve of water in the bulk state (top), confined in graphite pore (middle) and mica pore (bottom) of pore width of $H = 40$ Å at variable electric field strength: $E = 0$ (stars), 0.03 (diamonds), 0.1 (circles), and 0.20 V/Å (triangles). Open and filled symbols represent the coexistence densities and critical points, respectively. Error bars are of the order of the symbol size.

Figure 2. Vapor−liquid coexistence curve of water confined in graphite pore (top) and mica pore (bottom) of pore width of $H = 60$ Å at variable electric field strength: $E = 0$ (stars), 0.03 (diamonds), 0.1 (circles), and 0.20 V/Å (triangles). Open and filled symbols represent the coexistence densities and critical points, respectively. Error bars are of the order of the symbol size.

Figure 3. Variation in critical temperatures of bulk and confined water as a function of electric field. The open stars, diamonds, and circles correspond to the bulk water, confined water in graphite, and mica pore of width $H = 40$ Å, respectively. The left half-filled diamonds and circles symbols correspond to the water confined in graphite and mica pore of width $H = 60$ Å, respectively.

confirmed for water.[1,52] Additionally, middle and bottom curves of Figure 1 reveal a further decrease in the critical temperature of water confined in slit pores in the presence of an electric field. Interestingly, this drop in the critical temperature of confined water becomes more pronounced with increasing applied electric field strength. To understand the reason for this behavior, we analyze the saturated vapor−liquid densities of water in nanoconfinement. As indicated in Figure 1, water nanoconfined between graphite sheets exhibits a decrease in the liquid-phase density and an increase in the vapor-phase density with increasing electric field strength. Hence, the coexistence curve becomes narrow, leading to a reduction in the critical temperature and flattening of the vapor−liquid coexistence curve with increasing electric field strength, although the critical density remains largely unchanged. This observed trend is in contrast to the bulk thermodynamics of electrostriction in the absence of confining surfaces.[53,54] Density reduction under an applied electric field has previously been observed by Vaitheeswaran et al.[32] for water confined between narrowly separated graphite-like plates in an open system. As in the case of graphite, the liquid-phase density of water confined between
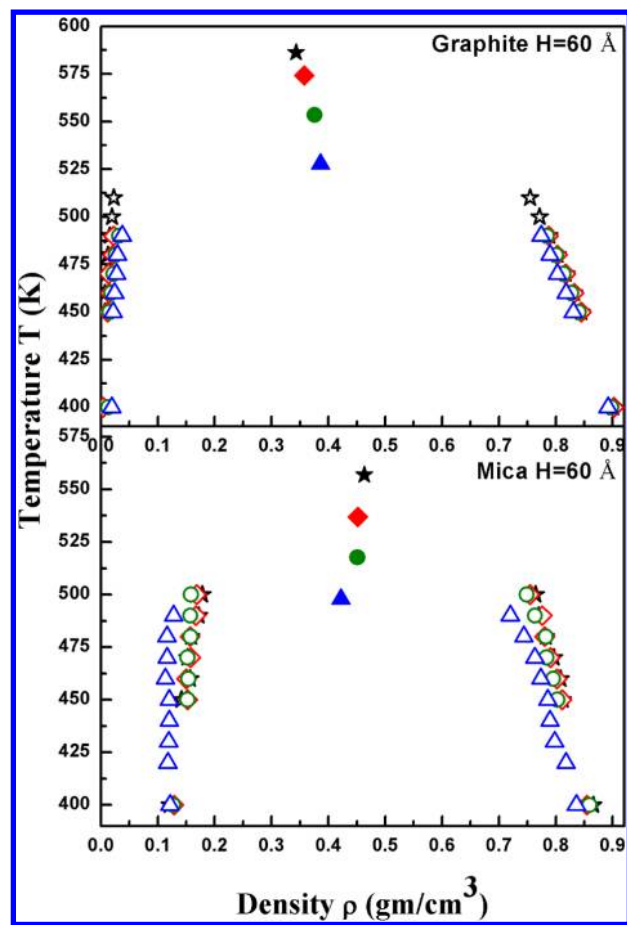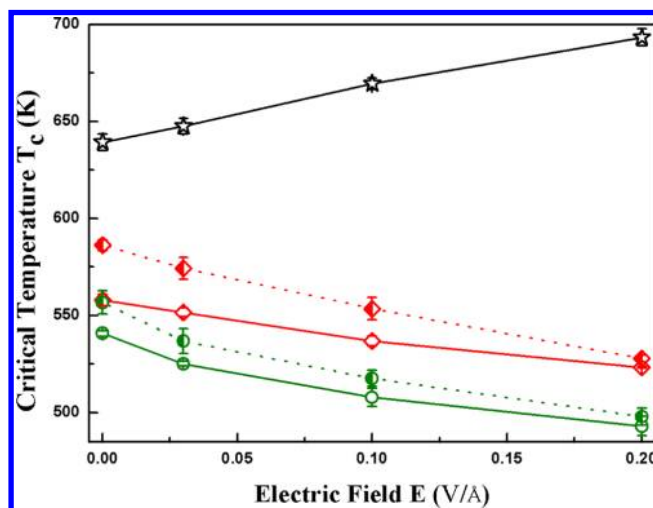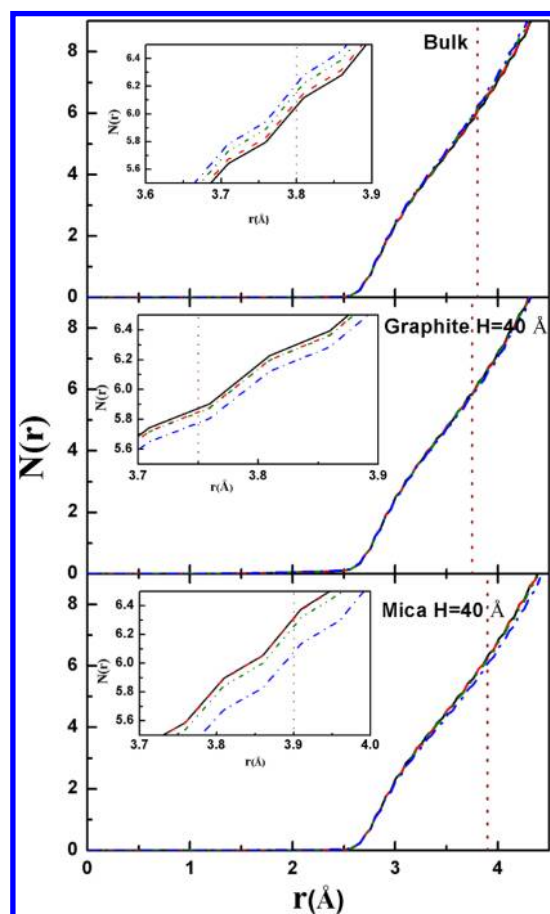
Table 2. Critical Temperature of Bulk and Confined Water at Different Electric Fields

electric field (V/Å)	critical temp (T_c) of bulk water (K)	critical temp (T_c) of confined water (K)			
		graphite pore (H = 40 Å)	mica pore (H = 40 Å)	graphite pore (H = 60 Å)	mica pore (H = 60 Å)
0.0	639 ± 4	558 ± 3	541 ± 2	586 ± 3	557 ± 6
0.03	648 ± 4	552 ± 2	525 ± 2	574 ± 6	539 ± 6
0.1	670 ± 3	537 ± 3	508 ± 5	554 ± 6	518 ± 4
0.2	693 ± 4	523 ± 2	493 ± 5	528 ± 2	498 ± 4

Figure 4. Coordination number $N(r)$ of the saturated liquid phase for varying electric field strength: $E = 0$ (black straight line), 0.03 (red dashed line), 0.1 (green dash-dot-dot line), and 0.20 V/Å (blue dash-dotted line), at $T = 450$ K, of bulk water (top), water confined in graphite (middle), and mica pore (bottom) of width $H = 40$ Å. The dotted vertical line represents the first coordination shell. Inset in panel shows zoomed image of coordination number near first coordination shell.

mica sheets decreases with increasing electric field, although only a minimal effect on the vapor-phase density is observed in this case (bottom curves of Figure 1).

The vapor−liquid-phase transition of water confined in graphite and mica materials with a large pore width ($H = 60$ Å) was also investigated; the respective results are shown in Figure 2. Water confined in large-width-pore graphite showed a similar trend as that in the case of the material with $H = 40$ Å—a decrease in the liquid-phase density and an increase in the vapor-phase density—with increasing electric field strength. In addition, we observed a lowering of the critical temperature, as
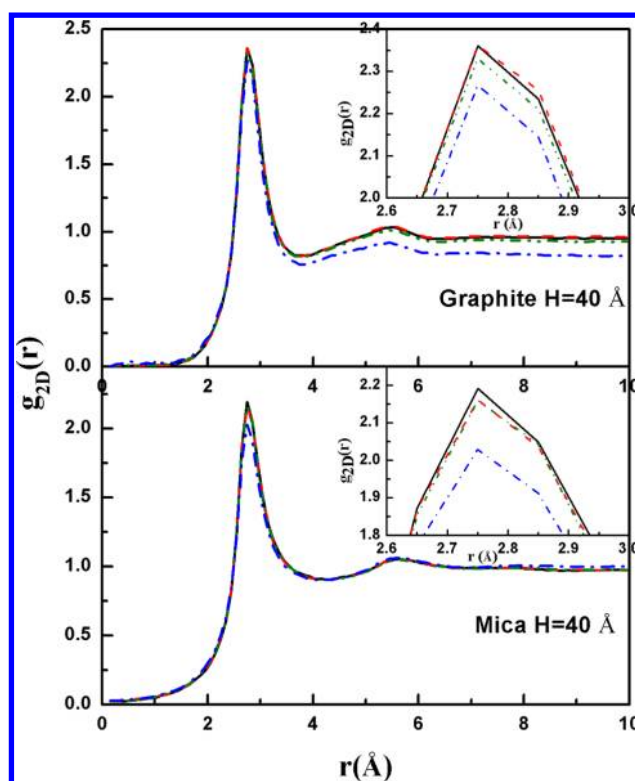
Figure 5. Two-dimensional radial distribution function, $g_{2D}(r)$, of saturated liquid phase of confined water layer near the surface of graphite pore (top) and mica pore (bottom) of width $H = 40$ Å, at $T = 450$ K, for different electric field strengths: $E = 0$ (black straight line), 0.03 (red dashed line), 0.1 (green dash-dot-dot line), and 0.20 V/Å (blue dash-dotted line). Inset shows the zoomed image of $g_{2D}(r)$ of confined water layer near the surface to the pore.

expected, although the critical density increased with the electric field. Similar to the case of graphite, the liquid-phase density of water confined in mica pores decreased with increasing applied electric field strength. The vapor-phase density, however, decreased with increasing electric field strength, thereby causing the critical density of water in large-width mica pores to decrease. The critical temperature showed a similar trend as in the case of graphite, and it decreased with increasing electric field strength. Figure 3 displays the effect of electric field on critical temperatures of bulk and confined TIP4P/2005 water. It is evident from Figure 3 that the dependence of critical temperature with varying electric field is quadratic in nature for bulk and confined water. However, the critical temperature of bulk water increases with the increasing electric field, whereas it follows an opposite trend in case of confinement. It is also noticed that suppression in critical temperature of confined water is more in the mica pore in comparison to the graphite pore. Similar evidence is also reported in our earlier work.[1] Table 2 summarizes the critical temperatures obtained in this work for confined water in mica and graphite pores with varying electric field.

As is evident from the vapor−liquid coexistence curve of bulk water (top curves of Figure 1), the liquid phase is found to be more sensitive to the presence of an electric field, as the liquid-phase density shows a noticeable increase with increasing electric field strength. This growing divergence between the liquid- and vapor-phase densities is typically attributed to the free energy barrier (or surface tension), which is known to increase with the electric field[55] for the bulk phase. In the case
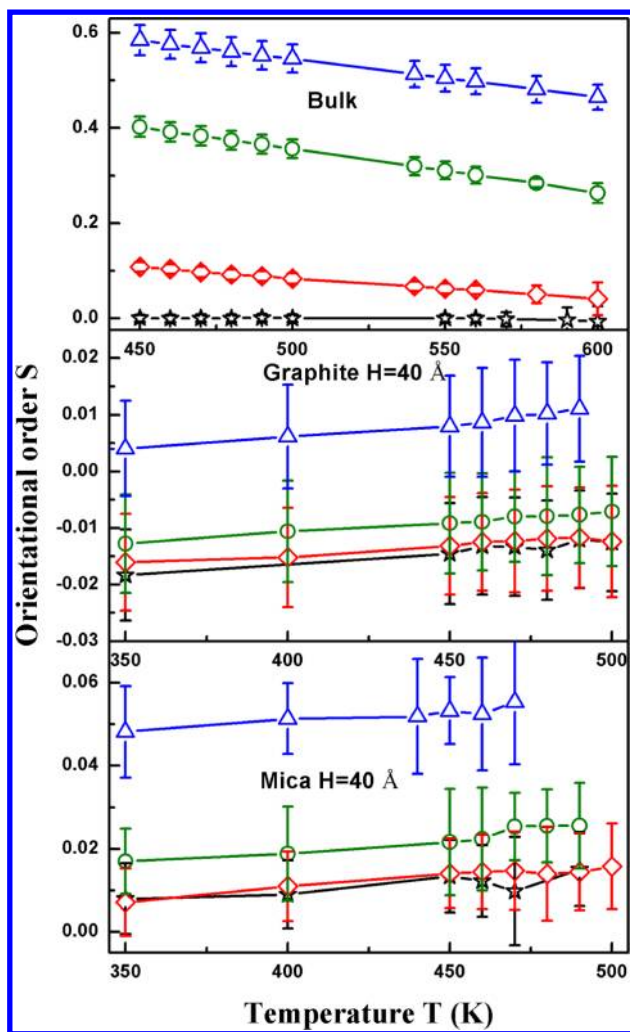
Figure 6. Orientational order parameter S of saturated liquid phase as a function of temperature for varying electric field strength: $E = 0$ (black stars), 0.03 (red diamonds), 0.1 (green circles), and 0.20 (blue triangles), of bulk water (top); water confined in graphite pore of width $H = 40$ Å (middle); water confined in mica pore of width $H = 40$ Å (bottom).

Figure 7. Distribution of the dipole vector orientation for saturated liquid phase of water in bulk (top), confined in graphite pore (middle), and mica pore (bottom) of width $H = 40$ Å at $T = 450$ K for varying field strength: $E = 0$ (black straight line), 0.03 (red dashed line), 0.1 (green dash-dot-dot line), and 0.20 V/Å (blue dash-dotted line).

of confined system, the liquid-phase density decreases, and the vapor−liquid coexistence envelope shrinks upon the application of an electric field. In order to understand this behavior, we examine several structural properties.

We first analyze the radial distribution function ($g(r)$) of water confined in graphite and mica pores. Our results show that overall $g(r)$ of liquid-phase water confined in hydrophobic (graphite) and hydrophilic (mica) pores (figures not shown) with a width of $H = 40$ Å is unaffected by the electric field. Similar observation have been reported for bulk water by Maerzke et al.[25] Nevertheless, we examined the effect of electric field on the overall coordination number, $N(r)$, of the liquid phase and is presented in Figure 4. It is clear from Figure 4 (top) that the $N(r)$ of bulk water increases with the electric field. On the other hand, $N(r)$ of liquid-phase water confined in graphite and mica pores with a pore width of $H = 40$ Å decreases with increasing electric field (see middle and bottom curves of Figure 4). In particular, $N(r)$ of liquid-phase water confined in the mica pore shows stronger dependence on the electric field than does that of water confined in the graphite pores. Similar trends are observed for the material with a pore
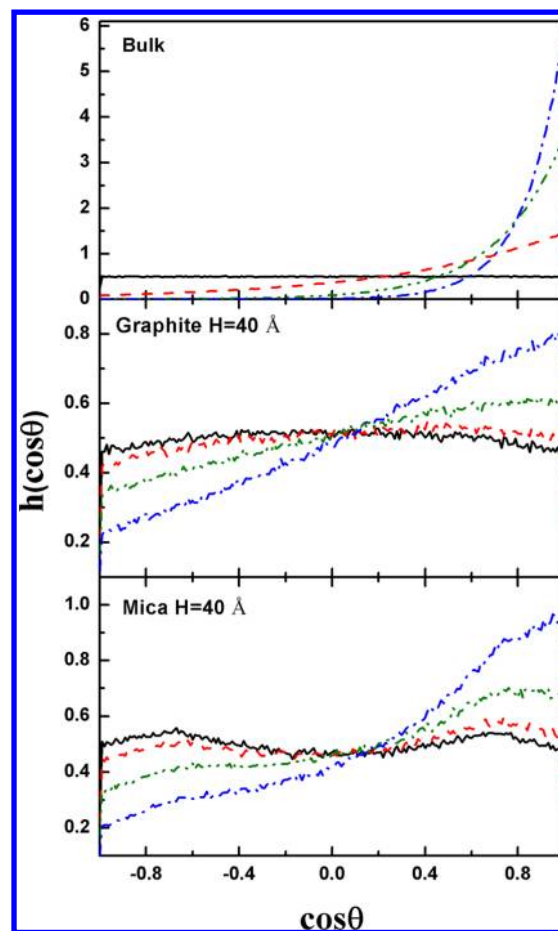
width of $H = 60$ Å (data not shown). As suggested by the increase in the critical temperature, $N(r)$ of bulk water increases with the electric field. The decrease in $N(r)$ can predict the observed decrease in the critical temperature in a confined environment, as indicated by the mean-field theory:[56]

$$T_c = c\frac{z\varepsilon}{k} \tag{8}$$

where c is a constant, z is the mean coordination number for a bulk molecule in the fluid, and ε is the energy of interaction with the nearest-neighbor molecule.

It is known that the presence of confining surface causes inhomogeneity in densities of confined water,[1] thereby forming layers near the pore surface. By extracting the information of different layers from density profile of confined water perpendicular to the surface, we have calculated in-plane radial distribution function, $g_{2D}(r)$, of layer near the surface and at the center of the pore. In Figure 5 (top) and (bottom), we have plotted $g_{2D}(r)$ of confined water layer near the surface of the graphite and mica pore, respectively. It can be seen from the figures that the first peak of $g_{2D}(r)$ of the surface layer of water decreases with the increase in electric field in both the cases (graphite and mica pores). Also, our analysis shows that the
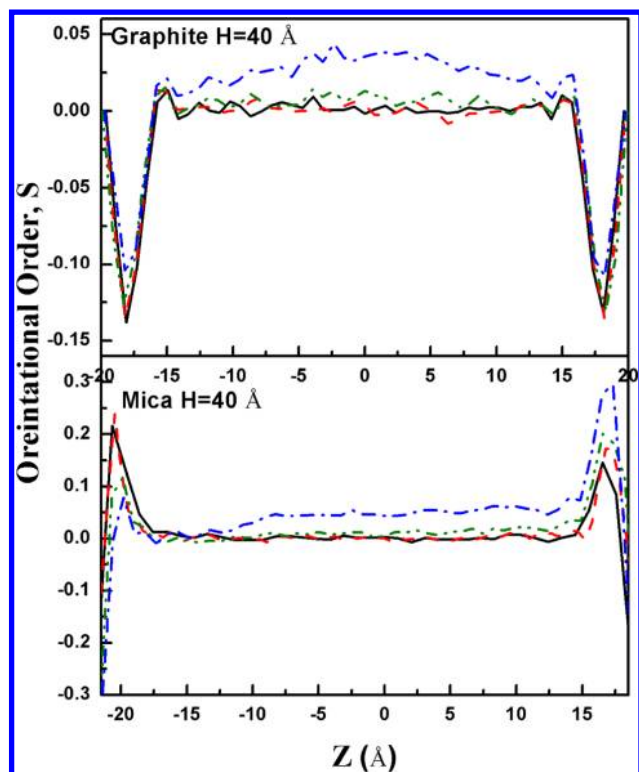
Figure 8. Orientational order profile of dipole vector of water confined in graphite pore (top) and mica pore (bottom) of width H = 40 Å at T = 450 K for varying electric field: E = 0 (black straight line), 0.03 (red dashed line), 0.1 (green dash-dot-dot line), and 0.20 V/Å (blue dash-dotted line).
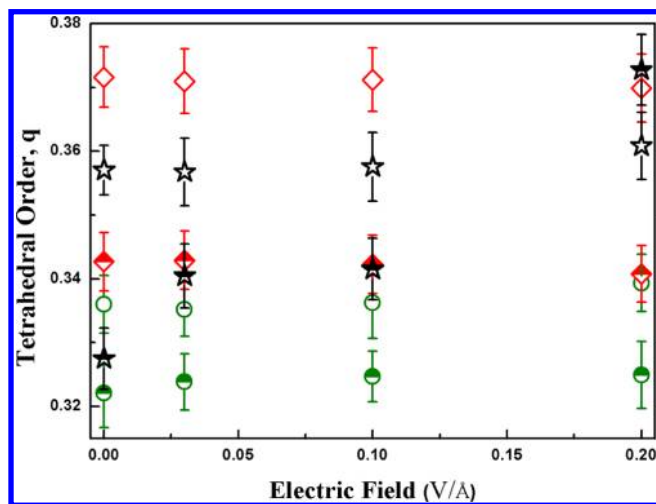

Figure 9. Tetrahedral order parameter q for the saturated liquid phase as a function of electric field strengths of bulk water (black stars); water confined in graphite pore of width H = 40 Å (red diamonds); water confined in mica pore of width H = 40 Å (green circles). Open and upper half-filled symbols are at temperatures T = 450 and 470 K, respectively.

effect of electric field on $g_{2D}(r)$ of confined water layer at the center of graphite and mica pores is negligible.

To understand the effect of the electric field on the orientation of confined fluids, we investigate the orientational order parameter (S), defined as

$$S = \frac{1}{2}\langle 3\cos^2\theta - 1\rangle \tag{9}$$

where θ is the angle between the electric field and the dipole vector. S approaches 1 for dipoles aligned with the field, -0.5 for dipoles perpendicular to the field, and 0 for dipoles with no preferential orientation. As shown in Figure 6, in the absence of an electric field, there is no preferential ordering in the liquid phase of bulk water, whereas in the presence of an electric field, there is now a competition between the hydrogen bond network and the tendency of the dipole vector of water molecules to align itself in the direction of the electric field. Nevertheless, increase in orientation is noticeable with increasing electric field strength. It can also be seen that at a constant electric field strength S decreases with an increase in temperature because of increased thermal fluctuations. This is in agreement with the results reported by Maerzke et al.[25] for the TIP4P water model. Middle and bottom curves of Figure 6 predict the ordering of liquid-phase water confined in hydrophobic (graphite) and hydrophilic (mica) pores (H = 40 Å), respectively. As compared to bulk water, the confined system shows considerable weak ordering even at the highest field strength (E = 0.2 V/Å) which may lead to the reduction of liquid phase density of confined water as suggested by England et al.[35] Although in a confined system there is a no preferential orientation of dipole under weak electric field, ordering increases slightly with an increase in electric field strength, as observed for E = 0.2 V/Å. Unlike the dipole vector of water confined in graphite, that of water confined in mica pores is oriented relatively more along the direction of the electric field. The magnitude of dipole ordering of confined water increases slightly at larger pore widths (H = 60 Å) (figure not shown) in graphite and mica pores.

To further examine the effect of the applied electric field on the orientational structure, the distribution of θ is calculated. A uniform cosine distribution is found for the liquid phase of bulk water in absence of the electric field (Figure 7). The dipole vector shows weak preference for an alignment parallel to the electric field at E = 0.03 V/Å, and this preference becomes stronger under a strong electric field (E = 0.2 V/Å). As in the case of bulk water, θ shows a uniform distribution in confined systems in the absence of the electric field, thereby indicating the randomness of the dipole vectors. Figure 7 (middle curves) presents the distribution of θ for water confined in graphite with a pore width of H = 40 Å. This distribution shows weak preference for parallel alignment at low electric fields (E = 0.03 V/Å), and this preference becomes stronger with increasing electric field strength. Similar to the case of graphite, the distribution of θ for water confined in mica indicates an increase in the parallel alignment with the applied electric field for the liquid phase (see Figure 7 (bottom)). Further, it can be seen that the tendency of the dipole vectors of water to align along the electric field decreases under confinement in comparison to bulk water (see Figure 7). Remarkably, the parallel alignment of the dipole vectors of water for mica increases as compared to that in the case of graphite. The distribution of θ parallel to the field increases with an increase in pore width to H = 60 Å (figure not presented). Further to this, the top and bottom panels of Figure 8 present the orientational order profile of the dipole vector of water confined in graphite and mica pore (of width H = 40 Å), respectively, in order to clarify the behavior of the orientational order of confined water near and away from the pore surfaces.
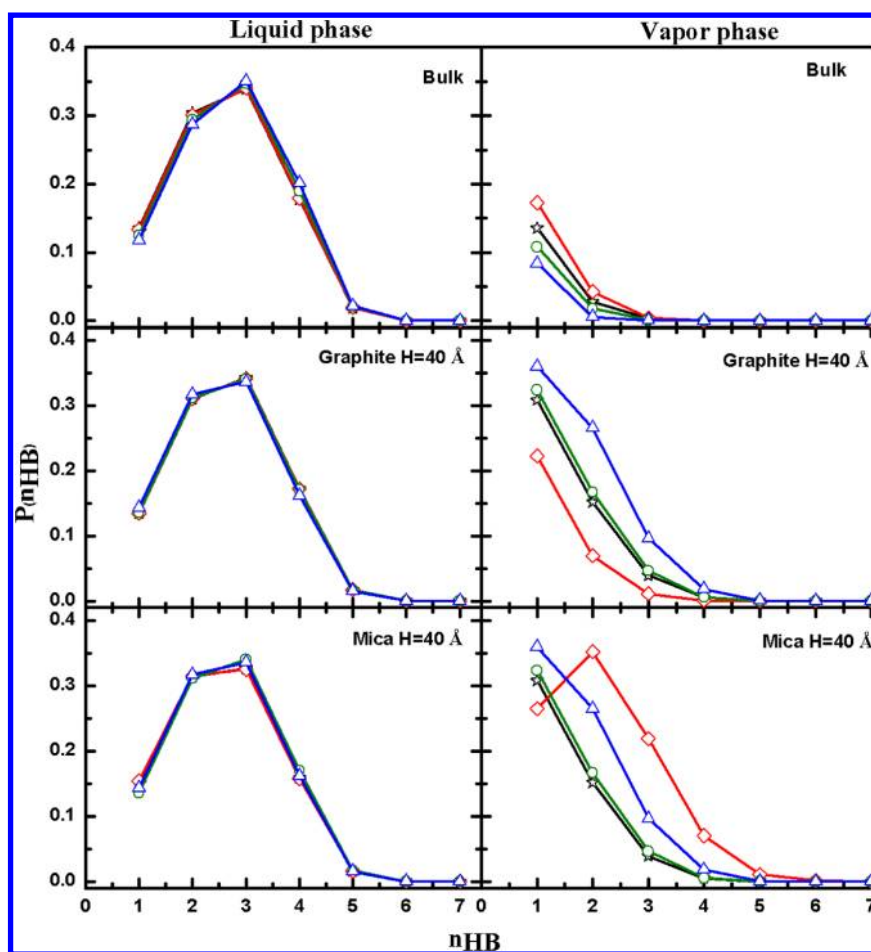
Figure 10. Normalized hydrogen bond distribution of water in bulk (top), confined in graphite pore (middle) and mica pore (bottom) of width $H = 40$ Å at $T = 450$ K for varying field strength: $E = 0$ (black stars), 0.03 (red diamonds), 0.1 (green circles), and 0.20 V/Å (blue triangles). Left and right panels are for saturated liquid phase and saturated vapor phase, respectively.

Figure 8 (top) suggests that the orientation of the dipole vector of confined water near the graphite surface is preferentially parallel to the direction of surface (i.e., perpendicular to the electric field direction), whereas in the case of mica pore (Figure 8 (bottom)), the dipole vectors near the pore surface tries to align themselves perpendicular to the surface (along the direction of electric field). The orientations of dipole vector are random at the center of the pore in both cases. The alignment of dipole vector in the direction of electric field increases with the increase in field strength. It can be also seen from the Figure 8 that the orientation of dipole vectors along the electric field direction near the lower mica surface decreases with increasing electric field strength, whereas it increase near the upper mica surface. This can be explained by the fact that mica surface has mobile K^+ ions, and oxygen likes to stay close to it with dipole vector pointing away from the surface. However, at other instances, where K^+ ion is absent, water molecule's hydrogen atoms are closer to the surface with oxygen atom away from the surface to maximize the hydrogen-bonding arrangement. The latter is the case for majority of the water molecules, which is evident from the orientation order profile at $E = 0$. With increasing E, hydrogen bonds network is bit frustrated and water dipole vector starts to orient toward the direction of the electric field. This means that the orientation order near the first surface of the pore should reach zero before decreasing further. For the other surface of the pore,

orientation order parameter should keep increasing toward 1. This is evident from the Figure 8. On the other hand, for the graphite surface only van der Waals (vdW) interactions play the role. Hence, electric field has to compete with hydrogen bonding among the water molecules, which is different from the case of mica surface where electric field competes additionally with the strong surface−water electrostatic interaction. This is what makes the two cases (graphite and mica pores) starkly different.

As indicated above, the orientational ordering of water is influenced by the applied electric field. However, the tetrahedral ordering of the confined water under the influence of the electric field has not been confirmed. Hence, we investigate the effect of the applied electric field on the tetrahedral ordering of bulk water and water under hydrophobic and hydrophilic confinement. The tetrahedral order parameter[57,58] (q) is defined as

$$q = 1 - \frac{3}{8} \sum_{j=1}^{3} \sum_{k=j+1}^{4} \left(\cos \phi_{jk} + \frac{1}{3} \right)^2 \tag{10}$$

where ϕ_{jk} is the angle between an oxygen atom and its nearest neighbors j and k.

q varies between 0 (ideal gas state) and 1 (perfect tetrahedral network). As shown in Figure 9, q of bulk water increases with the electric field strength at high temperatures, which is in
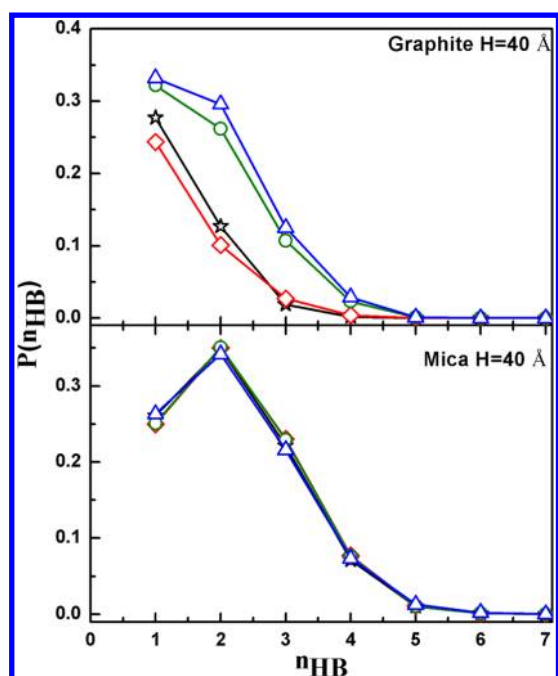
Figure 11. Normalized hydrogen bond distribution of water in vapor phase confined in graphite pore (top) and mica pore (bottom), of pore width $H = 60$ Å at $T = 450$ K, for varying field strengths: $E = 0$ (black stars), 0.03 (red diamonds), 0.1 (green circles), and 0.20 V/Å (blue triangles).

accordance with previous results reported by Maerzke et al.[25] Figure 9 also present the tetrahedral order parameter of water confined in graphite and mica pore ($H = 40$ Å). A very small deviation in q with increasing field strength is observed for water confined in these materials. It is interesting to note that although there is negligible change in q in the confined system, q decreases slightly with an increase in the field strength in case of graphite pores, whereas the opposite trend is seen in the case of mica pores. Similar trends are found for water confined in hydrophobic and hydrophilic pores with larger widths ($H = 60$ Å). In general, q of bulk and confined water decreases monotonically with increasing temperature at all field strengths due to the increase in randomness with the increase in temperature, which in turn results in the deformation of tetrahedrality and breaking of hydrogen bonds.

Discussion of hydrogen bonding (HB) is crucial in any investigation involving water. Therefore, we now consider the effect of the electric field on the hydrogen bonding of bulk and confined water. In particular, the effect of the electric field on HB in the coexisting phases of water molecules confined in hydrophobic and hydrophilic pores has remained unclear so far. Figure 10 presents the influence of the electric field on HB in the liquid (left panel) and vapor phases (right panel) of bulk water and confined water. It is found that the hydrogen-bonding network in the bulk water liquid phase is not significantly affected by the electric field. In the vapor phase of bulk water, however, a noticeable decrease in the extent of hydrogen bonding with increasing field strength is observed.

The middle and bottom curves of Figure 10 show HB in graphite- and mica-confined systems ($H = 40$ Å), respectively. The liquid phases do not show any significant change in hydrogen bonding, in the case of hydrophobic (graphite) and hydrophilic (mica) confinement. This behavior resembles that of bulk water. Unlike in the case of bulk water, the degree of

hydrogen bonding in vapor-phase water confined in graphite and mica pores increases with the electric field strength. At larger pore widths ($H = 60$ Å), the hydrogen-bonding network in the liquid phase is insensitive to the applied electric field strength, as in the case of smaller-pore-width materials. The extent of hydrogen bonding in vapor-phase water confined in graphite pores increases with the electric field, as in the case with $H = 40$ Å, although the effect of the electric field on the HB in vapor-phase water confined in mica pores is negligible. Thus, we can conclude that the liquid phase is saturated with HB and that this is reflected in the hydrogen bond distribution. However, for larger-pore-width ($H = 60$ Å) hydrophobic (graphite) materials, the HB in the vapor phase shows an interesting behavior: the HB increases with increasing electric field strength, resulting in higher vapor-phase density as shown in Figure 11. This behavior is not observed in the case of hydrophilic pores, as HB decreases slightly with increasing electric field strength.

4. CONCLUSIONS

We have investigated the influence of electric field strength on the vapor−liquid phase transition of water in bulk as well as in nanoconfinement states. We have also investigated the behavior of water in hydrophobic and hydrophilic confinement in the presence of an electric field. Our findings reveal that the application of an electric field increases the critical temperature of bulk water. This is mainly due to the increase in the density of the saturated liquid phase of bulk water in the presence of an electric field. Unlike the case of bulk water, the application of an electric field perpendicular to the confining surface decreases the liquid-phase density of the confined water film while increasing the evaporation rate.[13] As a result, the pore critical temperature of the confined water decreases. Additionally, it is noteworthy that the behavior of critical density in the presence of an electric field is different in hydrophobic and hydrophilic pores. With an increase in the electric field, the critical density increases in the hydrophobic (graphite) pores but decreases in the hydrophilic (mica) pores. This difference is mainly attributed to the difference in the HB nature in the vapor-phase water confined in hydrophobic and hydrophilic pores.

The first peak of $g_{2D}(r)$ liquid phase of confined water layer near the pore surface deceases with increase in electric field, whereas values of $g_{2D}(r)$ of confined water at the center of pore are found to be insensitive to the electric field. On the other hand, the observed changes in $N(r)$ for bulk and confined water in the presence of the electric field clearly indicate a difference in the behavior of critical temperature in these states. The increase in $N(r)$ of bulk water with the electric field results in a higher critical temperature. However, the decrease in $N(r)$ of water under confinement with increasing electric field suggests that the critical temperature shows the opposite behavior. The observed decrease in $N(r)$ of confined water upon the application of an electric field is more pronounced in hydrophilic pores than in hydrophobic pores. The parallel orientation of the dipole vectors increases with the electric field strength for bulk water. Confinement is found to increase the randomness of the dipole orientation of confined water even at strong field strengths. This effect is found to be more prominent in the hydrophobic pores than in the hydrophilic pores. The q value of bulk water is found to increase with increasing electric field, whereas this parameter remains almost unchanged for confined water. However, the application of a strong electric field causes a slight alteration in the q value of

confined water. Interestingly, q shows opposite behaviors in the presence of the electric field, depending on the nature of the pores (hydrophilic vs hydrophobic). We also analyzed the orientational order profile of water in hydrophobic and hydrophilic surface, and our results confirmed that the behaviors of dipole vector of confined water in mica and graphite pores are starkly different. The difference is primarily due the hydropillic nature of the mica surface (with mobile K^+ playing an important role). The strong surface water interaction (in mica pore) yields a higher vapor-like phase density of water in mica pores in comparison to that in graphite pores, which results in strong hydrogen bonding in the vapor phase.

■ AUTHOR INFORMATION

Corresponding Author
*E-mail: jayantks@iitk.ac.in.

Notes
The authors declare no competing financial interest.

■ ACKNOWLEDGMENTS

■ REFERENCES

(1) Srivastava, R.; Docherty, H.; Singh, J. K.; Cummings, P. T. *J. Phys. Chem. C* **2011**, *115*, 12448.
(2) Cummings, P. T.; Docherty, H.; Iacovella, C. R.; Singh, J. K. *AIChE J.* **2010**, *56*, 842.
(3) Singh, S. K.; Singh, J. K.; Kwak, S. K.; Deo, G. *Chem. Phys. Lett.* **2010**, *494*, 182.
(4) Huang, H. C.; Chen, W. W.; Singh, J. K.; Kwak, S. K. *J. Chem. Phys.* **2010**, *132*, 224504.
(5) Liu, Y.; Panagiotopoulos, A. Z.; Debenedetti, P. G. *J. Chem. Phys.* **2010**, *132*, 144107.
(6) Singh, S. K.; Singh, J. K. *Fluid Phase Equilib.* **2011**, *300*, 182.
(7) Singh, S. K.; Saha, A. K.; Singh, J. K. *J. Phys. Chem. B* **2010**, *114*, 4283.
(8) Brovchenko, I.; Oleinikova, A. *Interfacial and Confined Water*, 1st ed.; Elsevier: Amsterdam, 2008.
(9) Lin, L.; Pisano, A. P.; Lee, A. P. Microbubble Powered Actuator. *Transducers'91*, 1991.
(10) Takagi, H.; Maeda, R.; Ozaki, K.; Parameswaran, M.; Mehta, M. Phase Transformation Type Micro Pump. *Proceedings of the 5th International Symposium on Micro Machine and Human Science, Nagoya, Japan*, 1994.
(11) Bergstrom, P. L.; Ji, J.; Liu, Y.-N.; Kaviany, M.; Wise, K. D. *J. Microelectromech. Syst.* **1995**, *4*, 10.
(12) Yun, K.-S.; Yoon, E.; Leondes, C. T. *Micropumps for MEMS/NEMS and Microfluidic Systems*; Springer: New York, 2006; p 1112.
(13) Okuno, Y.; Minagawa, M.; Matsumoto, H.; Tanioka, A. *J. Mol. Struct. (THEOCHEM)* **2009**, *904*, 83.
(14) Li, D.; Xia, X. *Adv. Mater.* **2004**, *16*, 1151.
(15) Salata, O. V. *Curr. Nanosci.* **2005**, *1*, 22.
(16) Debye, P.; Kleboth, K. *J. Chem. Phys.* **1965**, *42*, 3155.
(17) Orzechowski, K. *Chem. Phys.* **1999**, *240*, 275.
(18) Beaglehole, D. *J. Chem. Phys.* **1981**, *74*, 5251.
(19) Early, M. D. *J. Chem. Phys.* **1992**, *96*, 641.
(20) Hegseth, J.; Amara, K. *Phys. Rev. Lett.* **2004**, *93*, 057402.
(21) Bateni, A.; Laughton, S.; Tavanaa, H.; Susnar, S. S.; Amirfazli, A.; Neumann, A. W. *J. Colloid Interface Sci.* **2005**, *283*, 215.
(22) Boda, D.; Winkelmann, J.; Liszi, J.; Szalai, I. *Mol. Phys.* **1996**, *87*, 601.
(23) Stevens, M. J.; Grest, G. S. *Phys. Rev. E* **1995**, *51*, 5976.
(24) Svishchev, I. M.; Hayward, T. M. *J. Chem. Phys.* **1999**, *111*, 9034.
(25) Maerzke, K. A.; Siepmann, J. I. *J. Phys. Chem. B* **2010**, *114*, 4261.
(26) Yeh, I.-C.; Berkowitz, M. L. *J. Chem. Phys.* **1999**, *110*, 7935.
(27) Zhang, G.; Zhang, W.; Dong, H. *J. Chem. Phys.* **2010**, *133*, 134703.
(28) Svischev, I. M.; Kusalik, P. G. *Phys. Rev. Lett.* **1994**, *73*, 975.
(29) Daub, C. D.; Bratko, D.; Leung, K.; Luzar, A. *J. Phys. Chem. C* **2007**, *111*, 505.
(30) Powell, M. R.; Cleary, L.; Davenport, M.; Shea, K. J.; Siwy, Z. S. *Nat. Nanotechnol.* **2011**, *6*, 798.
(31) Luo, J. B.; Shen, M. W.; Wen, S. Z. *J. Appl. Phys.* **2004**, *96*, 6733.
(32) Vaitheeswaran, S.; Yin, H.; Rasaiah, J. C. *J. Phys. Chem. B* **2005**, *109*, 6629.
(33) Bratko, D.; Daub, C. D.; Leung, K.; Luzar, A. *J. Am. Chem. Soc.* **2007**, *129*, 2504.
(34) Bratko, D.; Daub, C. D.; Luzar, A. *Phys. Chem. Chem. Phys.* **2008**, *10*, 6807.
(35) England, J. L.; Park, S.; Pande, V. S. *J. Chem. Phys.* **2008**, *128*, 044503.
(36) Zhu, S.-B.; Robinson, G. W. *J. Chem. Phys.* **1991**, *94*, 1403.
(37) Abascal, J. L. F.; Vega, C. *J. Chem. Phys.* **2005**, *123*, 234505.
(38) Koga, K.; Gao, G. T.; Tanaka, H.; Zeng, X. C. *Nature* **2001**, *412*, 802.
(39) Heinz, H.; Koerner, H.; Anderson, K. L.; Vaia, R. A.; Farmer, B. L. *Chem. Mater.* **2005**, *17*, 5658.
(40) Rothbauer, R. *Neues Jahrb. Mineral., Monatsh.* **1971**, 143.
(41) Plimpton, S. *J. Comput. Phys.* **1995**, *117*, 1.
(42) Gordillo, M. C.; Nagy, G.; Martí, J. *J. Chem. Phys.* **2005**, *123*, 054707.
(43) Rowlinson, J. S.; Swinton, F. L. *Liquids and Liquid Mixtures*, 3rd ed.; Butterworth: London, 1982.
(44) Rowlinson, J. S.; Widom, B. *Molecular Theory of Capillarity*; Clarendon: Oxford, UK, 1982.
(45) Swiatla-Wojcik, D. *Chem. Phys.* **2007**, *342*, 260.
(46) Aragones, J. L.; MacDowell, L. G.; Siepmann, J. I.; Vega, C. *Phys. Rev. Lett.* **2011**, *107*, 155702.
(47) Kirkwood, J. G.; Oppenheim, I. *Chemical Thermodynamics*; McGraw-Hill: New York, 1961.
(48) Frank, H. S. *J. Chem. Phys.* **1955**, *23*, 2023.
(49) Gonzalez, M. A.; Abascal, J. L. F. *J. Chem. Phys.* **2011**, *135*, 224516.
(50) Pi, H. L.; Aragones, J. L.; Vega, C.; Noya, E. G.; Abascal, J. L. F.; Gonzalez, M. A.; McBride, C. *Mol. Phys.* **2009**, *107*, 365.
(51) Gelb, L. D.; Gubbins, K. E.; Radhakrishnan, R.; Sliwinska-Bartkowiak, M. *Rep. Prog. Phys.* **1999**, *62*, 1573.
(52) Brovchenko, I.; Geiger, A.; Oleinikova, A. *J. Phys.: Condens. Matter* **2004**, *16*, S5345.
(53) Rasaiah, J. C.; Isbister, D. J.; Stell, G. *J. Chem. Phys.* **1981**, *75*, 4707.
(54) Shkel, Y. M.; Klingenberg, D. J. *J. Appl. Phys.* **1996**, *80*, 4566.
(55) Bateni, A.; Susnar, S. S.; Amirfazli, A.; Neumann, A. W. *Langmuir* **2004**, *20*, 7589.
(56) Givens, J. A.; Stell, G. Condensed Matter Theories. In *Condensed Matter Theories*; Blum, L., Malik, F. B., Eds.; Plenum: New York, 1993; Vol. *8*, p 395.
(57) Chau, P.-L.; Hardwick, A. J. *Mol. Phys.* **1998**, *93*, 511.
(58) Errington, J. R.; Debenedetti, P. G. *Nature* **2001**, *409*, 318.